Microporous and Mesoporous Materials 380 (2024) 113317

Contents lists available at ScienceDirect

Microporous and Mesoporous Materials

journal homepage: www.elsevier.com/locate/micromeso

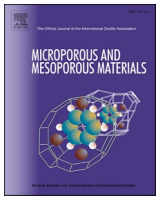

Structural stability and adsorption behaviour of CO_2-loaded pure silica CHA and ITW zeolites upon compression

G. Bera [a,*], P. Botella [a], J. Pellicer-Porres [a], D. Diaz-Anichtchenko [a], D. Errandonea [a], O. Gomis [b], R. Oliva [c], J. Ibañez [c], F. Alabarse [d], S. Valencia [e], F. Rey [e], A. Otero-de-la-Roza [f], D. Santamaria-Perez [a]

[a] Departamento de Física Aplicada-ICMUV, MALTA Consolider Team, Universitat de València, Valencia 46100, Spain
[b] Centro de Tecnologías Físicas: Acústica, Materiales y Astrofísica, MALTA Consolider Team, Universitat Politècnica de València, 46022 València, Spain
[c] Geociències Barcelona (GEO3BCN), CSIC, Lluís Solé Sabarís s/n, 08028 Barcelona, Spain
[d] Elettra Sincrotrone Trieste, Trieste 34149, Italy
[e] Instituto de Tecnología Química, Universitat Politècnica de València – Consejo Superior de Investigaciones Científicas, 46022, Valencia, Spain
[f] Departamento de Química Física y Analítica, Facultad de Química, MALTA Consolider Team, Universidad de Oviedo, Oviedo 33006, Spain

ARTICLE INFO

Keywords:
Zeolites
CO_2 adsorption
Structural phase transition
High pressure
EoS

ABSTRACT

The present study investigates the structural stability and adsorption behavior of ultrahigh CO_2-loaded pure-silica zeolites chabazite (CHA) and ITQ-12 (ITW) under high pressure conditions. To analyze these properties, we have utilized *in situ* synchrotron-based X-ray powder diffraction techniques. Lattice indexation provides information of the filling process and, through Rietveld refinements and Fourier recycling methods, we have been able to (i) determine the location and amount of guest carbon dioxide molecules within the cavities of pure-SiO_2 CHA zeolite and (ii) tentatively determine that within the channels of the porous pure-SiO_2 ITW framework. The filling of the zeolite pores with CO_2 molecules was found to have a positive impact on the structural stability of both CHA and ITW under compression, which do not undergo pressure-induced amorphization up to 12.2 GPa and 15.9 GPa, respectively. Interestingly, low compressibility takes place in CHA zeolite below 4 GPa during CO_2 loading and a second-order phase transition occurs in CO_2-filled ITW zeolite at 2.1 GPa. These results highlight the influence of CO_2 adsorption on the compressibility behavior of these zeolites. Overall, our study provides detailed insights into the structural behavior of CO_2-loaded CHA and ITW under high pressure and allows comparison with other pure silica zeolites described in the literature.

1. Introduction

The main anthropogenic greenhouse gas is carbon dioxide (CO_2). Its emission from human activities, primarily from burning fossil fuels, contributes significantly to global warming and climate change [1–3]. The reduction of CO_2 concentration in the atmosphere is therefore a pressing environmental issue [4–7]. Carbon capture and storage (CCS) strategies have emerged as reliable options for mitigating climate change worldwide [8,9]. Pure silica and aluminosilicate zeolite materials and membranes, in particular, are highly desirable for gas separation due to their uniform porosity, thermal and chemical stability, adjustable textural properties and ability to withstand pressure. They have shown potential as adsorbents for removing CO_2 from natural gas and biogas streams and accommodate CO_2 molecules within the structure [10–15]. The structure of zeolite materials plays a crucial role in CO_2 adsorption and separation from a gas mixture. Small-pore zeolitic membranes having eight-member rings (8 MR) are highly preferred in CO_2 capture processes due to the fact that their pore size (~3.8 Å in diameter) is close to the kinetic diameter of molecular CO_2 (3.3 Å) [16]. Over the years, the CO_2 capture performance of these materials has significantly improved, since the selection of pore size and topology in these zeolite compounds can maximize selectivity. Studies have shown that CO_2 interaction with the framework is enhanced in solids with larger framework density and closely-fitting pores, leading to improved separation [17–19]. Porous materials have revealed several separation mechanisms such as trapdoor adsorption, guest-induced flexibility, and molecular sieving [20–22]. The pore topologies of these materials can be classified as channel-like or cavity-like, with channel-like materials

* Corresponding author.
E-mail address: ganesh@uv.es (G. Bera).

https://doi.org/10.1016/j.micromeso.2024.113317
Received 25 June 2024; Received in revised form 21 August 2024; Accepted 26 August 2024
Available online 27 August 2024

having smaller variations in pore cross-sections in comparison to cavity-like materials and being more prone to closely fitting with the adsorbate [11]. Note that the pores must also be sufficiently large to allow for good interactions with the adsorbate through the molecular sieve effect, which can contribute to selectivity [23,24].

The determination of the amount of CO_2 stored in the cages and channels of open framework structures, the specific location of these CO_2 molecules, and the behavior of ultrahigh loaded zeolites is therefore an ongoing area of research. High density CO_2-filled systems can be obtained at high pressures (HP) and present some interesting physical properties. The chemical interaction between CO_2 and porous silica structures at high pressures and/or temperatures also provide information that could help in the design of potential effective long-term CO_2 sequestration strategies. Several experimental studies on the high-pressure structural stability of ultrahigh CO_2-filled zeolites have been recently reported [25, 26]. The total amount of adsorbed CO_2 molecules in the zeolite is a critical parameter for determining its compression behavior. It is worth noting that the usual compression mechanism of zeolites involves the collapse of the structures' empty cages and channels. This structural collapse is impeded by the presence of CO_2 guest molecules, which leads to the deactivation of the pressure-induced amorphization mechanism observed in the absence of guest species [27–29]. Interestingly, experiments conducted in diamond anvil cells (DACs) have shown a high concentration of adsorbed carbon dioxide in the LTA-type zeolite pores (CO_2/SiO_2 = 13/24) at 0.5 GPa, which is significantly greater than the adsorption value (CO_2/SiO_2 = 6–9/24) at 0.5 MPa and 303 K, as calculated from lower pressure CO_2 adsorption isotherm [25]. Another example of CO_2-filled silica zeolite which has gained attention due to its topology-related absorption properties is the MFI-type silicalite-1 zeolite. Its structure possesses unique straight and sinusoidal channels that enable the adsorption of CO_2 molecules at specific locations [30]. Initially, CO_2 molecules tend to occupy the straight channels, which are the most stable sorption sites at low loadings. As the loading increases, the guest molecules start occupying the sinusoidal pores and intersections. This behavior is attributed to van der Waals interactions between carbon dioxide and the framework atoms [30–33]. Experiments have demonstrated a maximum CO_2 adsorption capacity at 0.7 GPa, reaching a CO_2/SiO_2 ratio of 1/6 [26]. In these systems, the complete filling of pores by CO_2 molecules enhances structural stability under compression and significantly reduces the system's compressibility compared to the empty zeolite. The possibility of irreversible pressure-induced reconstructive phase transitions, as experimentally observed in other systems [34], could contribute to the development of potential long-term CO_2 sequestration strategies.

These findings highlight the need for further investigation into the behavior and properties of other CO_2-filled zeolite structures under high pressures and temperatures. In this study, we have investigated the adsorption performance of CO_2 upon compression in pure silica zeolite materials with small pores and different pore topologies [35]. By selecting materials with very small pore openings, we aim to exploit the molecular sieving effect, while materials with close-fitting pores offer the potential for a confinement effect. Our study focuses on the adsorption properties of CO_2 on a small pore pure silica CHA- and ITW-type zeolites. The hydrophobic nature of cation-free pure-silica zeolites makes them more moisture-resistant compared to the aluminium-containing ones [36].

The CHA-type zeolite, specifically pure-silica CHA, is a highly studied material known for its small pore size and uniform 3-dimensional pore structure. With a framework density of 15.1 [SiO_4] tetrahedra per 1000 Å^3, its rhombohedral $R\bar{3}m$(SG No. 166) structure consists of a piling of *t-cha* [$4^{12}6^28^6$] and *t-hpr* [4^66^2] building units. It has been extensively researched for its applications in CO_2/CH_4 and CO_2/N_2 separation as an adsorbent or membrane. Thus, it has gained popularity due to their strong molecular sieving ability, making them effective in separating CO_2 from CH_4 and N_2 [37,38]. The ITW-type zeolite, on the other hand, is a monoclinic $C2/m$ structure which has a channel-like topology with pores measuring 2.4 Å × 5.3 Å and 3.8 Å × 4.1 Å along the [100] and [001] directions, respectively [39]. This structure is characterized by a framework density of 17.7 [SiO_4] tetrahedra per 1000 Å^3. An interesting observation is that, having similar pore sizes to other pure silica adsorbents, ITW exhibits higher CO_2/CH_4 selectivity [11]. This emphasizes the importance of not only considering the adsorbent composition and pore size but also the topology of the material in separation processes.

By keeping in mind the above mentioned points, in this study, we aim to investigate the structural behavior of two CO_2-filled pure silica porous compounds with different topologies, CHA- and ITW- type zeolites, under compression. To achieve this, we conducted angle-dispersive synchrotron X-ray diffraction (XRD) experiments up to 12.2 GPa for CHA and 15.9 GPa for ITW at room temperature (RT). The experimental results are complemented by first-principles total-energy calculations, which provide insights into the structure considering the presence of guest CO_2 molecules within the host framework.

2. Experimental details

The micron-sized polycrystalline pure silica chabazite (CHA) and ITQ-12 (ITW) samples were prepared following these methods.

- Pure silica chabazite zeolite (CHA) was synthesized following a recipe based on a reported procedure [40]. In particular, tetraethylorthosilicate (TEOS) was added to an aqueous solution of the structure directing agent N,N,N-trimethyl-1-adamantammonium hydroxide (SDA1OH). The mixture was stirred during the required time in order to allow the evaporation of the ethanol formed during the hydrolysis of TEOS and the excess of water. An aqueous solution of HF was added and the mixture was manually homogenized. Finally, an aqueous suspension containing seeds of chabazite with a Si/Al ratio of 65 were also added (5 % of the total silica as seeds) in order to promote the crystallization. The molar composition of the gel was the following: SiO_2: 0.50 SDA1OH: 0.50 HF: $3H_2O$. The gel was crystallized in Teflon-lined stainless steel autoclaves at 423 K during three days in rotating conditions. The autoclaves were cooled down and the zeolite was recovered by filtration, washing with deionized water and drying at 373 K. The occluded organic material was removed by calcination at 853 K, leading to a highly crystalline chabazite zeolite sample with 2–3 μm cubic crystals, as was confirmed by XRD and SEM [see Fig. S1 in supplementary material]. Chemical analysis of the sample revealed a Si/Al ratio higher than 1000, confirming the siliceous composition of the zeolite.
- Pure silica ITQ-12 zeolite (ITW) was synthesized following a reported procedure [41,42] consisting of hydrolysing the appropriated amount of TEOS in an aqueous solution of the structure directing agent 1,3,5-trimethylimidazolium hydroxide (SDA2OH). The resulting mixture was stirred at room temperature until the ethanol produced during hydrolysis of TEOS and the required amount of water was evaporated. Then, an aqueous solution of HF was added to the gel, and the final mixture was manually homogenized. The final gel composition was: SiO_2: 0.56 SDA2OH: 0.56 HF: $7H_2O$. The crystallization was carried out in Teflon-lined stainless steel autoclaves at 448 K for 14 days in rotating conditions. The ITW zeolite was recovered by filtration and exhaustively washed with distilled water, and finally was dried at 373 K. The zeolite was submitted to calcination in air atmosphere at 973 K for 3 h in order to remove the occluded organic materials, leading to a highly crystalline pure silica ITW zeolite with a highly variable particle shapes and crystals sizes ranging between 2 and,30 μm, as was confirmed by XRD and SEM [11].

HP experiments were conducted using membrane-driven piston-cylinder DACs equipped with 500 μm culet diamonds. The rhenium

gasket was pre-indented to a thickness of 45 μm and a pressure chamber with a diameter of 300 μm was prepared. This high yield strength metal does not show chemical reactivity with CO_2 at low temperatures ($T <$ 1200 K) [43–45]. Two independent experiments were performed for CHA- and ITW-type samples. They were placed together with two ruby chips, which were used as an internal pressure gauge [46]. Besides the sample and ruby chips, the DAC was loaded with high-purity CO_2 using a Sanchez-Technologies gas loading machine. The loaded CO_2 act as a pressure transmitting medium and also diffuse into the zeolite cages and channels. Pressures derived from the CO_2−I phase EoS [47] are consistent with those obtained from the ruby luminescence. Angle-dispersive X-ray diffraction (XRD) measurements under HP-RT conditions were conducted at the Xpress beamline at the Elettra Synchrotron Radiation facility. A monochromatic X-ray beam with a wavelength of 0.4956 Å and a spot size of 80 μm in diameter was employed for the experiments. The diffracted patterns were captured using a PILATUS 3S 6M detector from DECTRIS, with a sample-detector distance of 939.50 mm, and LaB_6 was utilized as the standard calibrant for the measurements. The experimental set-up under high-pressure conditions is illustrated in Fig. 1 showing the diamond-anvil cell, with the pressure chamber (sample + ruby + CO_2), sampled by synchrotron X-rays. The XRD patterns were processed from raw to conventional 2θ intensity data using Dioptas software [48]. The indexing and refinement of the XRD patterns were carried out using the Unit Cell [49], Powder-Cell [50], and Fullprof program [51] packages.

3. Computational details

Density-functional theory calculations were carried out using basis sets of numerical atomic orbitals (NAO), as implemented in the Fritz Haber Institut ab initio materials simulation (FHIaims) package [52], which provides linear scaling with system size [53]. In all calculations, the B86bPBE functional was used [54,55] in combination with the exchange-hole dipole moment (XDM) model for dispersion [56–58]. The B86bPBE-XDM functional has demonstrated excellent performance in the description of non-covalent interactions in solids [59]. We used the "light" basis set to describe the Kohn-Sham orbitals, corresponding to a double-ζ basis set, which has been shown to be adequate for the calculation of lattice energies [59]. All geometry relaxations were carried out using the Broyden-Fletcher-Goldfarb-Shanno (BFGS) optimization algorithm with a maximum force threshold of 0.005 eV/Å and a tight self-consistent field (SCF) convergence threshold for the electron density of 10^{-7} atomic units.

A preliminary exploration using the experimental structures was conducted to determine the k-point grid for each structure. k-point grids of 2 × 1 × 2 (ITW) and 2 × 2 × 2 (CHA) are enough to converge the total energy well below 1 meV per formula unit. The equilibrium geometries with various numbers of carbon dioxide molecules within the unit cell were relaxed at fixed constant pressure. In the case of CHA, the CO_2 molecules were placed at the positions suggested by our experimental determination. The location of the CO_2 molecules in ITW were determined by a geometry relaxation at zero pressure.

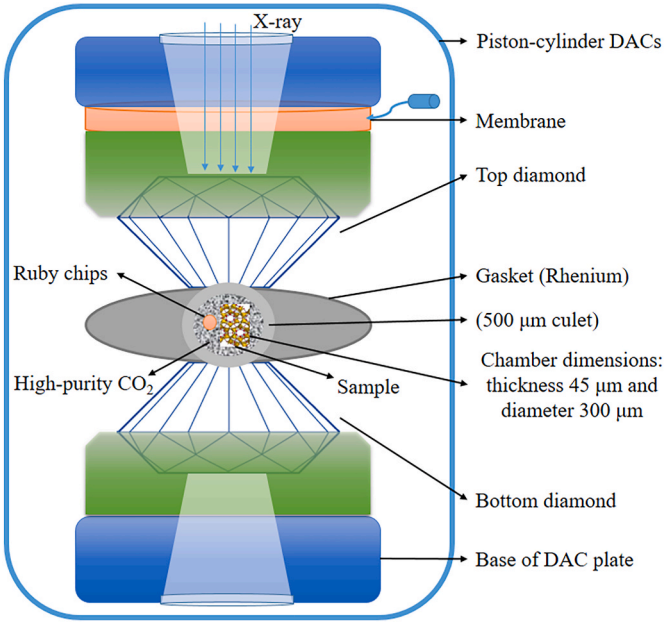

Fig. 1. Schematic diagram of the experimental set-up presenting membrane driven DACs having diamonds with 500 μm culets. The pressure chamber contains the zeolite sample, a small ruby chip as internal pressure gauge and high purity CO_2 as pressure transmitting medium (PTM), and it is sampled by the synchrotron X-rays.

4. Data analysis and results

In this manuscript the data analyses and results are presented separately in two subsections corresponding the CO_2-loaded silica CHA and ITW zeolites in order to understand adsorption behavior of carbon dioxide as a function of pressure in quite different framework topologies. A comparison between the results of both experiments will be done in the Summary and Conclusions section.

4.1. CO_2-loaded pure-SiO_2 CHA structure and its compressibility

The pressure-dependent structural behavior has been studied through synchrotron radiation XRD measurements. Fig. 2 displays the selected XRD patterns of the CO_2-loaded pure silica CHA zeolite at different pressures, ranging from 1.55 to 12.2 GPa. Upon initial observation, it is noted that there is no occurrence of a first-order structural phase transition throughout the entire pressure range, as evidenced by the absence of any appearance of diffraction peaks and the smooth displacement of the diffraction peaks. Additionally, there is no

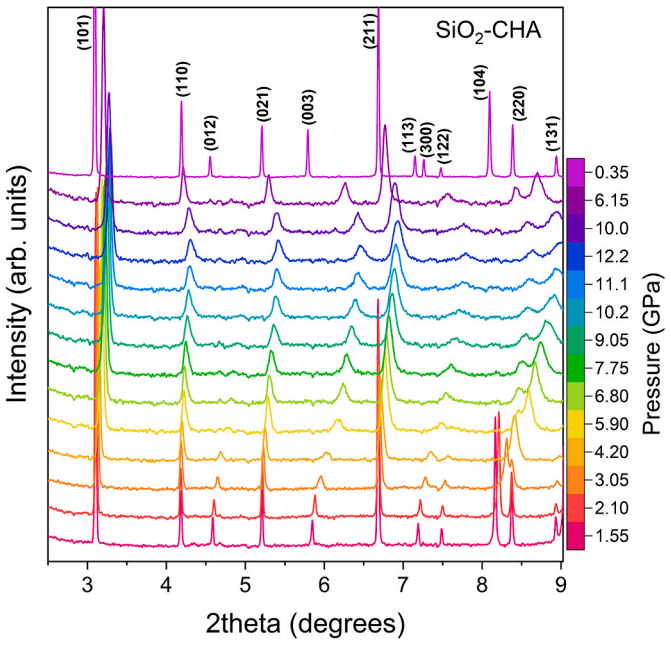

Fig. 2. Pressure dependent powder X-ray diffraction patterns of CO_2 loaded pure-SiO_2 CHA zeolite up to 12.2 GPa (λ = 0.4956 Å). No signature of pressure induced amorphization (PIA) exists up to highest measured pressure. The measured pressure range covered in the experiment is displayed in the colour bar at the right-hand side. Pressure uncertainty is estimated to be 0.05 GPa below 10 GPa and 0.1 GPa above that pressure.

indication of pressure-induced amorphization (PIA) at the highest pressure of 12.2 GPa, which would suggest the filling of the zeolite's pores by CO_2 molecules. Above 4.2 GPa XRD diffraction peaks broaden noticeably as a consequence of the deterioration of the quasi-hydrostatic conditions provided by solid CO_2-I PTM. On the other hand, as the pressure on the material increases, the peak intensities in the XRD patterns decrease and some of the peaks begin to merge together, becoming broader and slightly asymmetric. This phenomenon might be caused by local distortions within the crystal structure. However, although the patterns obtained at the highest pressures are of limited quality, from profile fitting it can be concluded that the initial rhombohedral phase of the CHA zeolite remains stable up to the maximum pressure investigated in this study. The profile analyses using structural descriptions based on $R\bar{3}m$ subgroups did not give a noticeably better fit.

The unit cell volume and lattice parameters collected in Table 1 have been obtained from peak indexing and exhibit a smooth variation with pressure as shown in Figs. 3 and 4, respectively. The behavior of the lattice parameters upon compression can be divided into two regions: (i) a low-pressure region, below ~3.7 GPa, where CO_2 loading in the host framework is completed, but the reorientation of CO_2 and accommodation of the corner-linked tetrahedral [SiO_4] zeolite structure is still taking place and the axes increase slightly (*a* axis below ~2 GPa) or decrease more slowly than expected (*a* axis from ~2 to ~3.7 GPa and *c* axis up to ~3.7 GPa), and (ii) a high-pressure region above 3.7 GPa, where the lattice parameters decrease smoothly upon compression, and the intensity of the (012) and (122) reflections has almost vanished above 4.2 GPa (see Fig. 2). This drastic reduction of intensity of these reflections is due, as discussed later, to a small displacement of the [SiO_4] tetrahedra causing the systematic extinction of these reflections. Beyond this pressure, the *P-V* dataset can be explained by a third-order Birch-Murnaghan equation of state (EoS) [60].

The EoS perfectly fitted our data (Fig. 3) above ~3.7 GPa. The graph does not show any volume discontinuity within the studied pressure range up to 12.2 GPa. The resulting EoS parameters are as follows: a zero-pressure volume (V_0) = 2545 (29) Å^3, a bulk modulus (B_0) = 24 (4) GPa, and a bulk modulus first pressure derivative (B'_0) = 5.2 (7). These experimental EoS parameters for CO_2-loaded pure-silica CHA zeolite are listed in Table 2 together with those predicted computationally for a similar loading content. It is noteworthy that the unit cell volume of the zeolite increases by approximately 8 % when CO_2 is adsorbed, as inferred from the RP-RT unit cell volume data of the empty CHA

Table 1
Lattice parameters and unit cell volumes of CO_2-loaded pure-SiO_2 CHA zeolite at different pressures obtained by peak indexing.

P (GPa)	a (Å)	c (Å)	V (Å^3)
10^{-4} (RP)	13.529 (6)	14.748 (8)	2338 (2)
1.55	13.570 (4)	14.578 (7)	2325 (2)
2.10	13.579 (4)	14.495 (7)	2315 (2)
2.65	13.573 (4)	14.386 (7)	2295 (2)
3.05	13.570 (4)	14.308 (7)	2282 (2)
3.70	13.555 (4)	14.214 (7)	2262 (2)
4.20	13.541 (4)	14.138 (7)	2245 (2)
4.75	13.514 (4)	14.040 (7)	2221 (2)
5.90	13.457 (4)	13.830 (7)	2169 (2)
6.35	13.443 (5)	13.715 (6)	2147 (2)
6.80	13.423 (5)	13.670 (6)	2133 (2)
7.20	13.395 (5)	13.612 (6)	2115 (2)
7.75	13.369 (5)	13.558 (6)	2098 (2)
8.35	13.335 (5)	13.485 (6)	2077 (2)
9.05	13.288 (4)	13.426 (6)	2053 (2)
9.65	13.266 (4)	13.355 (6)	2036 (2)
10.2	13.259 (4)	13.305 (6)	2026 (2)
10.6	13.218 (4)	13.277 (6)	2009 (2)
11.1	13.193 (4)	13.241 (6)	1996 (2)
11.7	13.161 (4)	13.194 (6)	1979 (2)
12.2	13.125 (4)	13.171 (6)	1965 (2)
0.35	13.559 (5)	14.721 (7)	2344 (2)

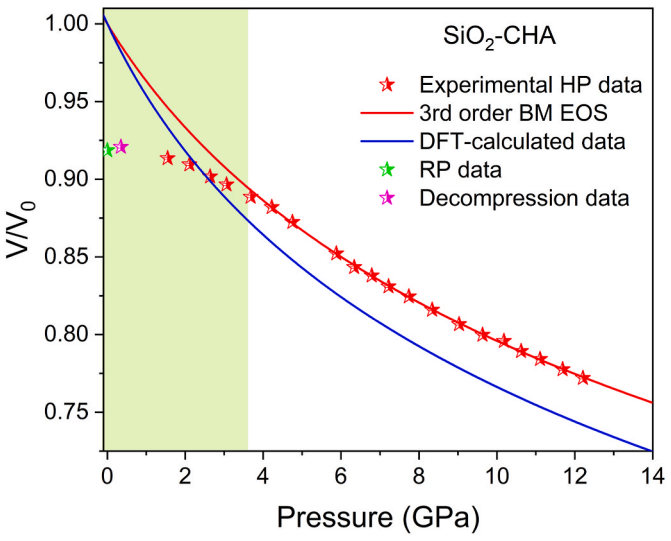

Fig. 3. P−V/V_0 data per formula unit of CO_2 loaded pure-SiO_2 CHA sample obtained from experiment and theoretical calculation. Red star symbols refer to experimental data points upon increasing pressure. Error bars are smaller than symbol size. The red solid line represents the fit to experimental data for 3.75 < P < 12.2 GPa with a third-order Birch−Murnaghan EoS. The blue solid line corresponds to the DFT calculated data for the same amount of loaded CO_2 molecules per unit cell with B'_0 = 7.4 (4).

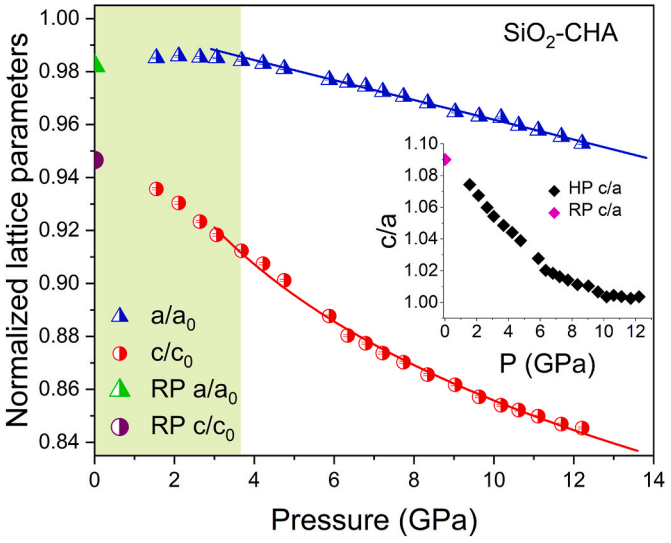

Fig. 4. Relative lattice parameters of CO_2 loaded pure-SiO_2 CHA framework under high pressure. Blue triangles represent the experimental data points of a/a_0 and the solid blue line is fitted data with second order isotherm BM EoS. Red circles show the experimental data points of c/c_0 and the solid red line is the fitted data of third order BM EoS. a_0 and c_0 values were obtained from the extrapolation of the fitting for P > 3.75 GPa data. Inset of the figure illustrates c/a ratios with pressure.

Table 2
Fitted parameters of the 3rd-order Birch-Murnaghan EoS for CO_2-loaded pure-SiO_2 CHA zeolite.

Parameters	Equation of state (EoS) for SiO_2-CHA	
	Experimental	DFT Calculated
V_0	2545 (29)	2292 (20)
B_0	24 (4)	11 (1)
B'_0	5.2 (7)	7.4 (4)

structure (see Tables 1 and 2). The obtained bulk modulus in this study is slightly smaller than those observed for other pure silica zeolite (LTA) filled with CO_2 ($B_0 = 39$ (3) GPa, and $B'_0 = 3.3$ (3)) [25] and silicalite zeolites filled with other atoms or molecules such as Ar ($B_0 = 35.9$ (4) GPa, $B'_0 = 4.7$ (5)) [61] or ammonia borane ($B_0 = 39.1$ (3) GPa, $B'_0 = 4$ (fixed)) [62]. Additionally, the compressibility behavior of CO_2-filled Si-CHA is comparable to that of other ultrahigh CO_2-filled pure-silica zeolite such as silicalite-1 ($B_0 = 26$ (4), $B'_0 = 5.5$ (7)) [26]. No compressibility data were experimentally obtained in the present work for the empty zeolite. However, reported data in other zeolite frameworks show that the complete filling of the pores, in an equilibrium process with the excess of guest species outside the pores which act as a pressure transmitting medium, substantially decrease the compressibility [63]. This is confirmed by DFT calculations on empty CHA, which predict a rapid distortion of the structure with the collapse of the cages and a bulk modulus of ~3 GPa.

The pressure evolution of the lattice parameters plotted in Fig. 4 shows that the *c* axis is most compressible. A linearization of the 2nd-order Birch-Murnaghan EoS (through the substitution of the volume for the cube of a lattice parameter) was used to analyze the axial compression [64], providing evidence of the strong anisotropy in this compound. Thus, the bulk moduli values obtained from data between 4 and 10 GPa are $B_a = 50$ (2) GPa and $B_c = 15.3$ (7) GPa, for the *a* and *c* axes, respectively, which indicate that the *a* axis is prominently more uncompressible and that the bulk compressibility is mainly dominated by that of the *c* axis.

In order to determine the quantity and exact location of the guest CO_2 molecules inside the pure silica CHA framework we conducted Rietveld refinement and Fourier difference map analyses at the lowest pressure (1.55 GPa). At this pressure, the structure can be described by a rhombohedral $R\bar{3}m$ space group and lattice parameters, $a = 13.570$ (4) Å and $c = 14.578$ (7) Å, as obtained from a LeBail refinement. Fig. 5a shows the Rietveld refinement of the experimental CO_2-loaded CHA XRD pattern using the empty CHA structure as model. It can be seen that the intensity of the calculated pattern does not match the experimental one particularly at 2θ angles above 6.5°. The change in peak intensity ratios between empty and the observed zeolite patterns and the aforementioned unit cell volume and the large stability of the host framework structure upon compression suggest the existence of carbon dioxide in the cages. Then, we assumed that the atomic coordinates of the host have not changed significantly between the empty structure at ambient pressure and the CO_2-filled structure at 1.55 GPa, and performed Rietveld refinement and Fourier recycling to locate the CO_2 molecules in the cages of the porous structure. This process is visually summarized in Fig. 6: (i) Fig. 5(left) represents the projection of the empty zeolite structure along the *c* axis, (ii) Fig. 5(middle) shows the Fourier difference map (*xy* plane) for unit cell summed along the *c* axis, and (iii) Fig. 5 (right) represents the same projection of the CO_2-filled zeolite structure. The best fitting was achieved with the insertion of ~13.5 CO_2 molecules per unit cell (occupation factors were refined). The atomic coordinates of the C and O atoms, together with the positions of the Si and O atoms of the host framework, are collected in a cif file of the Supplementary Material (see Table S1). This structure considerably improves the observed-calculated peak intensity ratios and the overall model refinement, showing good agreement with experimental data (see Fig. 5b). The framework topology and the location of CO_2 molecules within this framework is comparable but slightly different to that reported by Pham and coworkers for a low-loaded pure-silica CHA structure (5.5 molecules per unit cell) [17].

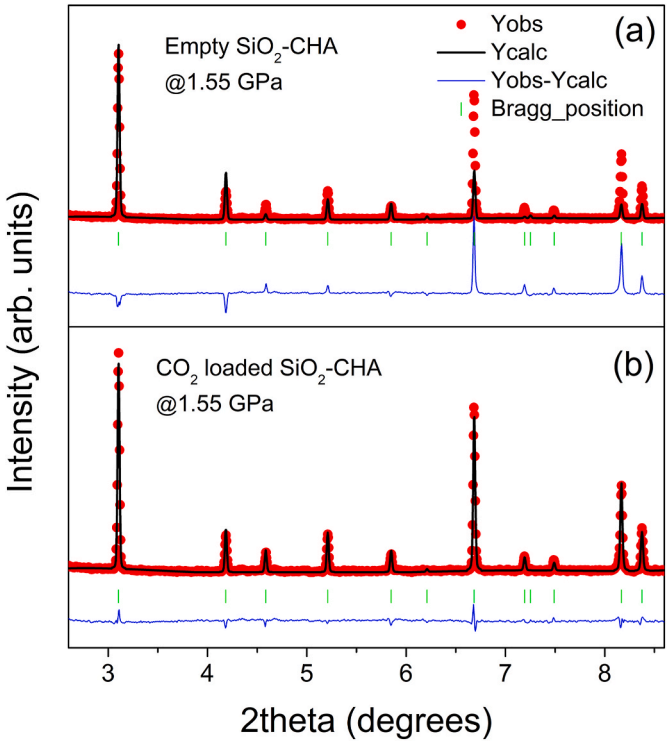

Fig. 5. Rietveld refinement of XRD pattern of CO_2 loaded pure-SiO_2 CHA sample at 1.55 GPa (a) fitted with an empty SiO_2 CHA framework model (Refined parameters: $R_p = 50$, $R_{wp} = 57$, $R_e = 43$ and $\chi^2 = 1.76$) and (b) fitted with a SiO_2 CHA framework filled with guest CO_2 molecules in which the occupation factor of CO_2 molecules is refined (Refined parameters: $R_p = 13.3$, $R_{wp} = 24$, $R_e = 42.4$ and $\chi^2 = 0.32$).

Fig. 2 shows clear changes in the relative intensities of the reflections upon compression. A Rietveld refinement of the XRD pattern at 5.9 GPa confirms a slight rearrangement of the host framework. This leads to a reduction in relative intensities as mentioned earlier. However, the quality of the XRD pattern refinement does not allow definitive conclusions to be drawn. Fig. S2 and the cif file provided as Supplementary Material shows the Rietveld refinement (at 5.9 GPa) and the atomic positions (see Table S2).

Once we have determined the existence of 13.5 CO_2 molecules per hexagonal unit cell it is interesting to discuss the density of CO_2 inside the pores. The pore volume in the CHA zeolite is 0.30 cm^3/g at ambient pressure, estimated from Ar adsorption [11]. We assume that the pore volume follows the same pressure behavior than the volume of the unit cell. Then the pore volume at 1.55 GPa would be roughly the same than in ambient conditions. The CO_2 density would then be 0.92 g/cm^3, smaller to the density of liquid CO_2 (1.3 g/cm^3 [65]) and much smaller than the density of solid CO_2 (1.8 g/cm^3 [>66]) at this pressure. The phase diagram of CO_2 suggests that CO_2 should be solid at 1.55 GPa. Several arguments could be invoked to explain why CO_2 would have smaller density than the solid. The first hypothesis is that pressure is not adequately transmitted to the CO_2 molecules in the pores. This hypothesis can be rejected on the basis that a pressure difference would induce the collapse of the zeolite, whereas the diffraction pattern does not indicate so. In second place, there could be not enough space in the pores for the molecules to adopt the configuration of solid CO_2. In third place, the thermodynamics of CO_2 molecules in the pores is in principle different from that of macroscopic CO_2, due to size effects. As a final consideration, we point out that even at the largest pressure attained, near 12 GPa, the estimated CO_2 density (near 1.09 g/cm^3) is still smaller than that of the solid.

Therefore, from the above discussion, we can say that the CHA framework possesses three-directional cavities with small size circular pores that have a diameter of approximately 3.8 Å, which is comparable to the dimensions of CO_2 molecules (3.3 Å) and this characteristic makes pure-SiO_2 CHA zeolite an effective adsorbent for carbon dioxide molecules upon compression.

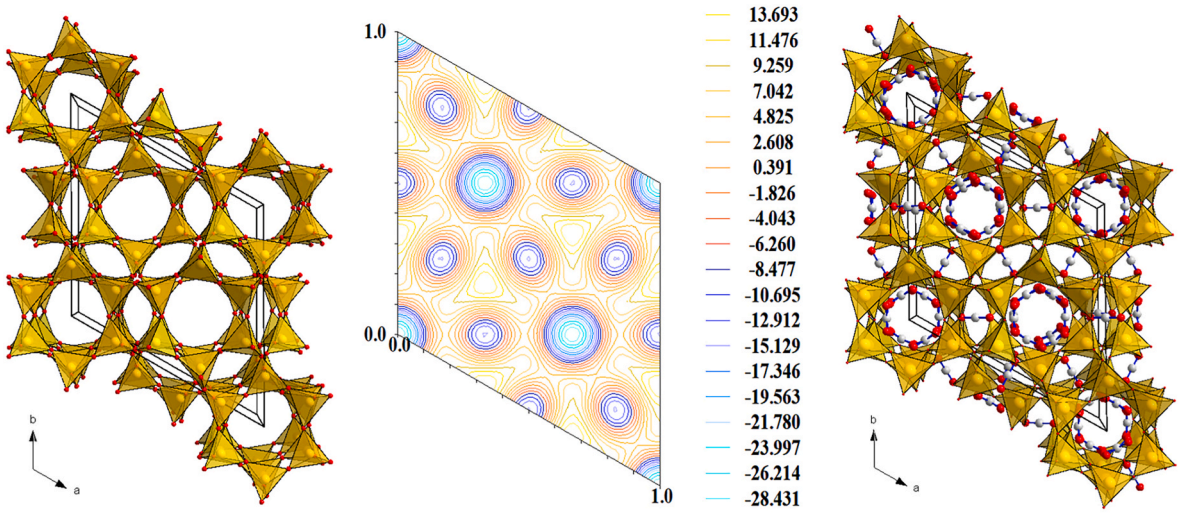

Fig. 6. (left) The projection of empty pure-SiO_2 CHA zeolite framework structure based on corner-connected [SiO_4] tetrahedral groups, (middle) Bidimensional difference fourier map perpendicular to the c axis in CO_2-filled CHA framework calculated using X-ray structure factors and (right) View of the CO_2-loaded pure-SiO_2 CHA structure along the c axis showing the location of CO_2 molecules at 1.55 GPa. Yellow, gray, and red spheres represent Si, C, and O atoms, respectively.

4.2. CO_2- loaded pure-SiO_2 ITW structure and its compressibility

Fig. 7 illustrates the pressure-dependent XRD patterns of the CO_2-loaded SiO_2-ITW sample up to the pressure of 15.9 GPa. The figure indicates clear evidence of a structural phase transition above 2.1 GPa, as observed through the appearance of diffraction peaks at different d-spacing. At this pressure, the pattern shows the coexistence of both phases. Above 2.6 GPa the second phase remains stable up to the maximum pressure reached in this study. Note that, even at the highest pressure, there is no evidence of pressure-induced amorphization (the low-2θ-angle X-ray diffraction lines are still relatively sharp at 15.9 GPa), due to filling of the pores by CO_2 molecules. The crystal system and unit cell parameters of the new phase observed at 2.6 GPa were determined through peak indexing of the XRD pattern, which indicates a transition to another monoclinic phase with slightly larger *c*-axis value. From that pressure onwards, the experimental XRD patterns can be explained by a monoclinic phase-II (as indicated in Fig. 8) with the same space group (SG: *C2/m*). Table 3 collects the indexed lattice parameters of CO_2-filled pure-SiO_2 ITW at all measured pressures. The equation of state (EoS) of the ITW compound obtained above 2.6 GPa differs significantly from those estimated in DFT calculations assuming a loading of 5 CO_2 molecules per unit cell, as shown in Fig. 9. Third-order Birch-Murnaghan equations of state fitted our experimental and theoretical data, giving the characteristic parameters collected in Table 4.

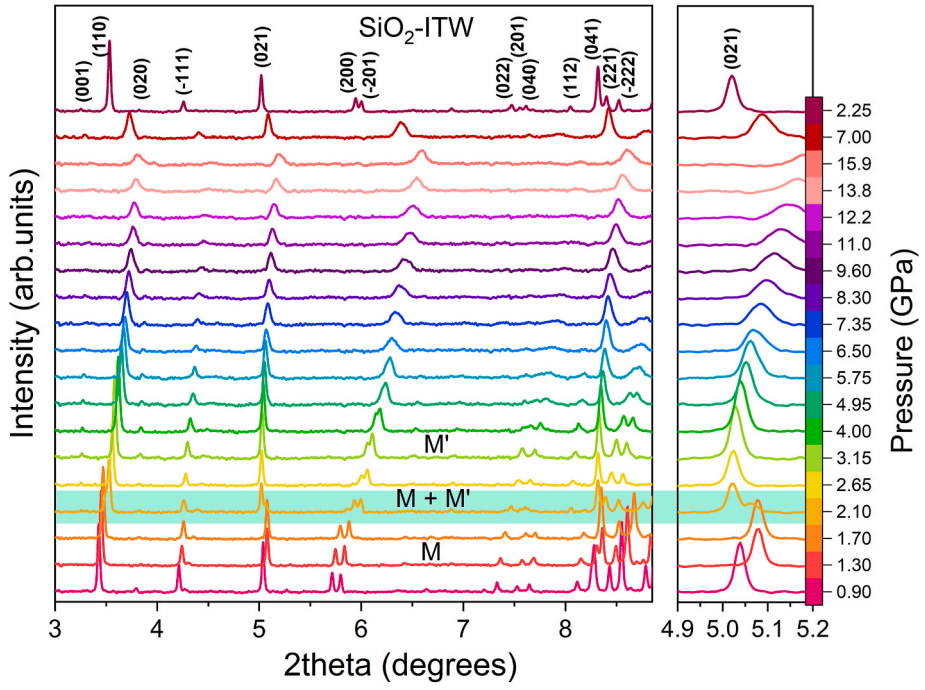

Fig. 7. Powder X-ray diffraction patterns of CO_2-loaded pure-SiO_2 ITW zeolite up to 15.9 GPa (λ = 0.4956 Å). As pressure increases, some peaks start to merge together and shift to the lower 2θ regions as the structure changes from monoclinic phase-I (M) to distorted monoclinic phase-II (M′) at 2.1 GPa. For pressures above 5 GPa, the peaks broaden suggesting a pressure-induced loss of crystallinity. Nevertheless, there is no signature of pressure induced amorphization (PIA) up to the highest measured pressure. The measured pressure range covered in the experiment is displayed in the colour bar on the right-hand side.

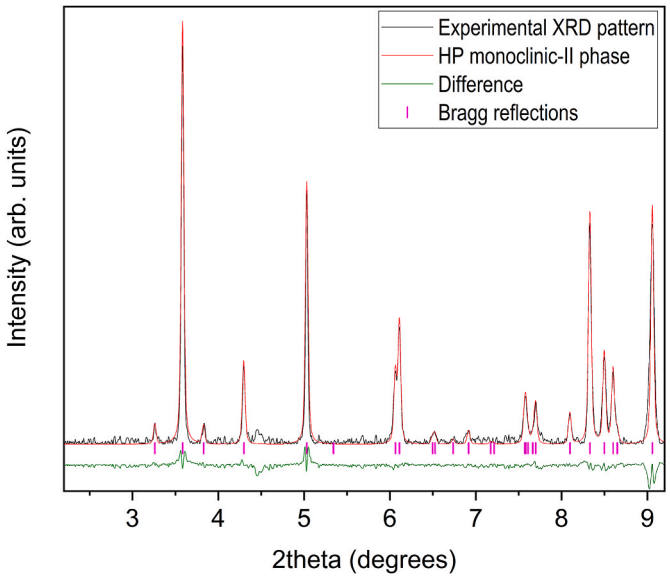

Fig. 8. LeBail refinement of the XRD pattern of CO_2 loaded pure-SiO_2 ITW sample at 3.15 GPa with the monoclinic C2/m phase-II.

Table 3
Lattice parameters and unit cell volumes of CO_2-loaded pure-SiO_2 ITW zeolite at different pressures obtained from peak indexing.

P (GPa)	a (Å)	b (Å)	c (Å)	β (°)	V (Å^3)
10^{-4} (RP)	10.336 (5)	15.018 (16)	8.864 (8)	105.35 (4)	1327 (1)
0.90	10.310 (4)	14.989 (16)	8.880 (6)	105.24 (4)	1323 (1)
1.30	10.247 (4)	14.806 (16)	8.843 (6)	105.21 (4)	1294 (1)
1.70	10.161 (4)	14.845 (16)	8.818 (6)	105.27 (4)	1284 (1)
2.10	10.093 (4)	14.867 (16)	8.834 (6)	105.35 (4)	1279 (1)
2.10	9.902 (4)	14.855 (9)	9.024 (6)	104.83 (4)	1283 (1)
2.65	9.783 (4)	14.847 (9)	9.019 (6)	104.79 (4)	1267 (1)
3.15	9.694 (4)	14.839 (9)	9.005 (6)	104.77 (4)	1253 (1)
3.55	9.623 (4)	14.816 (9)	8.992 (6)	104.69 (4)	1240 (1)
4.00	9.563 (4)	14.802 (9)	8.985 (6)	104.68 (4)	1230 (1)
4.55	9.503 (4)	14.778 (9)	8.977 (6)	104.67 (4)	1220 (1)
4.95	9.463 (4)	14.762 (9)	8.963 (6)	104.69 (4)	1211 (1)
5.30	9.429 (4)	14.754 (9)	8.955 (6)	104.63 (4)	1205 (1)
5.75	9.395 (4)	14.725 (9)	8.955 (6)	104.69 (4)	1198 (1)
6.23	9.375 (4)	14.708 (9)	8.950 (6)	104.48 (4)	1195 (1)
6.50	9.347 (4)	14.690 (9)	8.949 (6)	104.48 (4)	1190 (1)
6.80	9.331 (4)	14.679 (9)	8.931 (6)	104.37 (4)	1185 (1)
7.35	9.290 (4)	14.673 (10)	8.908 (10)	104.61 (4)	1175 (1)
7.75	9.263 (4)	14.670 (10)	8.851 (10)	104.58 (5)	1164 (1)
8.30	9.231 (4)	14.649 (10)	8.863 (10)	104.57 (5)	1160 (1)
9.00	9.203 (4)	14.593 (10)	8.879 (10)	104.30 (5)	1156 (1)
9.60	9.158 (4)	14.578 (9)	8.886 (10)	104.29 (5)	1150 (1)
10.3	9.125 (4)	14.563 (9)	8.858 (10)	104.31 (5)	1141 (1)
11.0	9.097 (4)	14.547 (9)	8.827 (10)	104.29 (5)	1132 (1)
11.4	9.081 (4)	14.538 (9)	8.784 (10)	104.38 (5)	1123 (1)
12.2	9.042 (4)	14.496 (9)	8.812 (10)	104.23 (5)	1120 (1)
13.2	9.021 (4)	14.455 (9)	8.768 (10)	104.39 (5)	1107 (1)
13.8	9.001 (4)	14.407 (9)	8.773 (10)	104.23 (5)	1103 (1)

The obtained EoS parameters are $V_0 = 1366$ (19) Å^3, $B_0 = 23$ (7) GPa, and $B'_0 = 11$ (3) resulting in a bulk modulus (B_0) comperable with CHA but a higher B'_0 value. The P-V/V_0 graph also suggests the presence of two different axial compressibility regimes for the CO_2-loaded pure-SiO_2 ITW zeolite: (i) for pressures below 2.6 GPa, and (ii) for pressures above 2.6 GPa. In both cases, the axial compressibility is slightly anisotropic, the *a* axis being more compressible than the *b* and *c* axes beyond 2.6 GPa (see Fig. 10). We employed the linearization of a 2nd-order BM EoS [64] to model the lattice parameters in the 4–10 GPa pressure range. The axial bulk moduli of the *a*, *b* and *c* axes are $B_a = 23.3$ (7) GPa, $B_b = 103$ (3) GPa and $B_c = 90$ (9) GPa, respectively.

To investigate the adsorption behavior of CO_2 molecules within the

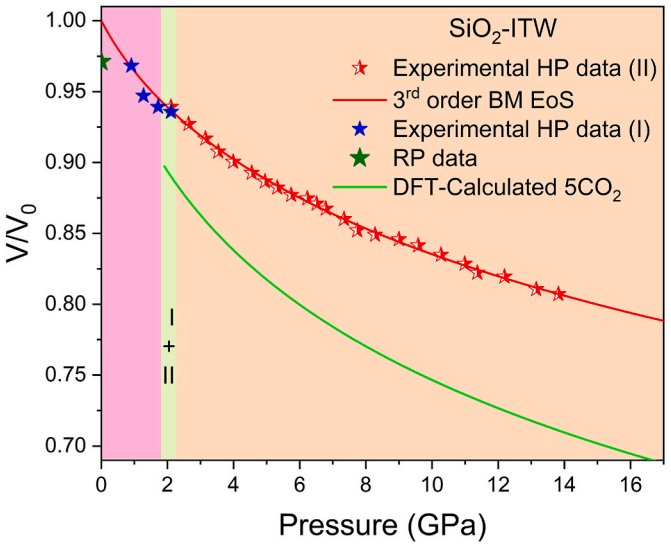

Fig. 9. P−V/V_0 data per formula unit of CO_2 loaded pure-SiO_2 ITW zeolite. Blue (Phase-I) and red (Phase-II) star symbols refer to experimental data points. Error bars are smaller than symbol size. The red solid line represents the fit to the experimental data with a third-order Birch−Murnaghan EoS. The green solid line corresponds to DFT calculated data fitted with third-order Birch−Murnaghan EoS corresponding to 5 CO_2 molecules per unit cell.

Table 4
Fitted parameters of the 3rd-order Birch-Murnaghan EoS for CO_2-loaded pure-SiO_2 ITW zeolite.

Parameters	Equation of state (EoS) of ITW	
	Experimental	DFT Calculated (5CO_2)
V_0	1366 (19)	1266 (14)
B_0	23 (7)	11.6 (2)
B'_0	11 (3)	8 (0)

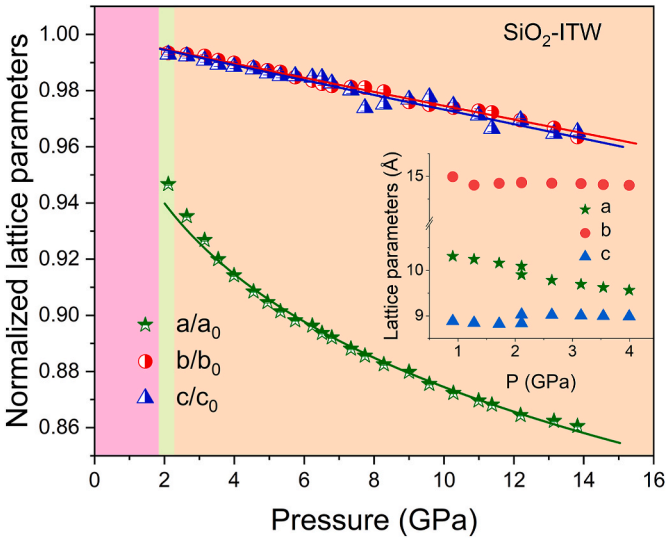

Fig. 10. Relative lattice parameters of CO_2 loaded pure-SiO_2 ITW framework under high pressure. Green stars, blue triangles and red circles represent the experimental data points of a/a_0, b/b_0 and c/c_0, respectively, and the solid lines are the fitted data with second order BM EoS. Inset of the figure shows the variation of lattice parameters with pressures carrying absolute values.

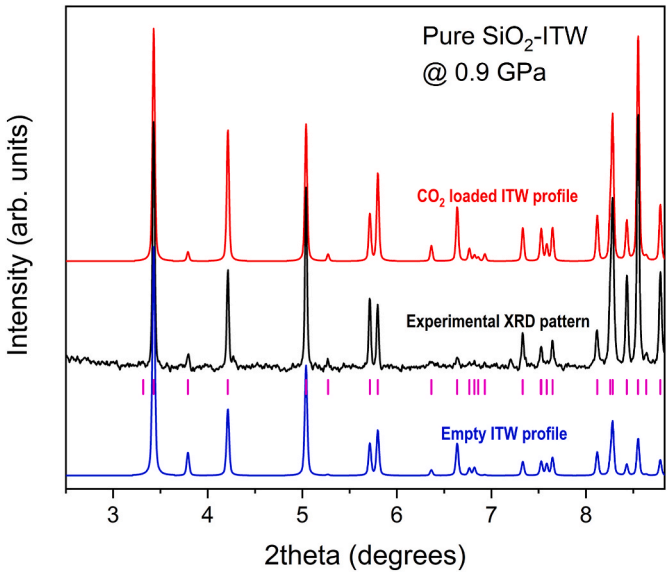

Fig. 11. Experimental XRD pattern of CO_2-loaded pure-SiO_2 ITW zeolite at 0.9 GPa (center, in black) together with calculated X-ray diffraction profiles of both, the empty ITW framework (bottom, in blue) and the filled-ITW zeolites with guest CO_2 molecules tentatively obtained from the Fourier map calculation (top, in red).

pure-SiO_2 ITW framework, the Rietveld refinement technique was employed using XRD data at a lowest measured pressure, 0.9 GPa (see Fig. 11). Initially, the refinement was performed on the empty ITW structure having monoclinic symmetry (SG: *C*2/*m*), but the fitting did not match the experimental data accurately, particularly at higher 2θ angles (See Fig. 10, bottom), due to CO_2 filling. The positions of the CO_2 molecules were tentatively determined by analyzing the difference-Fourier maps, but the powder data are of limited quality. The number of the guest CO_2 molecules was only estimated, refining the occupation factor and keeping other parameters fixed except the scale factor until the best fit to the data was obtained. When CO_2 molecules were considered in the refinement, a better agreement between the fitting and experimental data was achieved (Fig. 10, top). The refined occupation factor revealed that there are approximately 4.5 CO_2 molecules per unit cell in the pure-SiO_2 ITW framework. The tentative atomic coordinates of the C and O atoms of carbon dioxide are given in the Supplementary Material (see Table S3). The crystal structure of the empty ITW, Fourier map and CO_2-loaded ITW compounds are depicted in Fig. 12. Therefore, these static high-pressure results suggest the existence of an ultrahigh CO_2-loaded ITW structure with ~4.5 CO_2 molecules per unit cell at 0.9 GPa. Interestingly, a similar estimation of the CO_2 density as the one performed with the CHA zeolite yields different results. Considering 4.5 CO_2 molecules per unit cell and a pore volume of 0.18 cm^3/g (ambient conditions, Ref. [11]), a CO_2 density of 0.76 g/cm^3 is readily obtained. In the case of the ITW zeolite the obtained density is smaller than that of liquid CO_2. This is related to the smaller framework channels, which forces the CO_2 molecules to be aligned.

5. Summary and Conclusions

The present study investigated the detailed structural behavior of CO_2-loaded pure-silica CHA and ITW zeolites under room-temperature high-pressure conditions. The results provided insights into the adsorption process, the location of CO_2 molecules within the zeolite framework, and their phase stability. The presence of CO_2 molecules within the zeolite frameworks influenced the phase stability and adsorption process differently in each case. While CO_2 hindered denser phase formation in CHA zeolite, an isostructural phase transition occurred at 2.6 GPa in ITW zeolite. Pressure-induced amorphization was prevented by CO_2 adsorption in both cases up to the highest measured pressure. This behavior can be explained by the existence of two cooperative effects: (i) the mechanical impossibility of collapse due to the existence of CO_2 guest molecules in cages and channels of CHA and ITW zeolites, the difference of pressure between the exterior of the zeolite and the pores is much smaller than the applied pressure, which prevents the reduction of volume. Additionally, the solidification of CO_2-I partially suppresses the porosity which prevents amorphization, and (ii) the flexibility of the zeolites under compression, based mainly on tilting of rigid tetrahedra around the sharing corners of the [SiO_4] units that behave as hinges. P-induced tilting of tetrahedra usually leads to a continuous rearrangement of the framework. The study revealed that approximately 13.5 CO_2 molecules were accommodated in the cavities of the pure-SiO_2 CHA structure per unit cell at 1.55 GPa, with a CO_2 density similar to liquid CO_2. ITW zeolite accommodated 4.5 CO_2 molecules per unit cell at 0.9 GPa, in the framework channels, where the CO_2 density would be smaller than that of the liquid. The number of CO_2 molecules in the unit cell is fairly consistent with the extrapolation[1] of the adsorption isotherms of CO_2 measured up to 700 KPa at ambient temperature to our pressure, with an estimated content of 12.9 molecules in the CHA and 4.8 CO_2 molecules within ITW framework. Fig. 13 shows the adsorption isotherms of CO_2 at room temperature with the extrapolated adsorption isotherm at low pressure for CHA and ITW [11] and the CO_2 adsorption content of present studied at the lowest pressure. The loading capacity as defined by a CO_2/SiO_2 ratio was determined to be 3/8 for CHA zeolite which is smaller than those of other zeolites with larger pores and cavities, such as the LTA-type that can accommodate 13/24 molecules of CO_2 per SiO_2 molecule [25] or the RHO-type that has considered to host as much as one CO_2 molecule per SiO_2 molecule [[>67]]. On the other hand, the CO_2/SiO_2 ratio was 4.5/24 for ITW zeolite, a value very similar to that found in Silicalite-1 (1/6 ratio), whose porous structure has a comparable framework density (18.4 [SiO_4] tetrahedra per 1000 $Å^3$) having straight and sinusoidal channels [26]. The compressibility behaviors of the both CO_2-loaded zeolites exhibited peculiarities at low pressures, with CHA zeolite showing anomalously low compressibility below about 4 GPa and ITW zeolite undergoing a phase transition at 2.6 GPa. The bulk moduli of both compounds were comparable, but the ITW bulk modulus rapidly increased with pressure ($B'_0 = 11$ (3)). Such a strong increase in bulk modulus could be related to the compressibility nature of the CO_2-filled channels, which would contrast to that of the CO_2-filled large cavities in CHA zeolite. Overall, this research provides valuable insights into the behavior of high-CO_2-loaded zeolite structures under high-pressure conditions, highlighting differences in phase stability and adsorption processes between CHA and ITW zeolites.

CRediT authorship contribution statement

G. Bera: Writing – review & editing, Writing – original draft, Supervision, Methodology, Investigation, Conceptualization. **P. Botella:** Writing – review & editing, Methodology. **J. Pellicer-Porres:** Writing – review & editing, Methodology, Conceptualization. **D. Diaz-Anichtchenko:** Writing – review & editing. **D. Errandonea:** Writing – review & editing. **O. Gomis:** Writing – review & editing, Methodology. **R. Oliva:** Writing – review & editing. **J. Ibañez:** Writing – review & editing. **F. Alabarse:** Writing – review & editing, Methodology. **S. Valencia:** Writing – review & editing, Methodology. **F. Rey:** Writing – review & editing, Methodology. **A. Otero-de-la-Roza:** Writing – review & editing, Methodology, Investigation. **D. Santamaria-Perez:** Writing – review & editing, Supervision, Methodology, Investigation, Conceptualization.

[1] This extrapolation is based on its asymptotic behavior at low pressures [11], which was fitted by a two-phase exponential growth function.

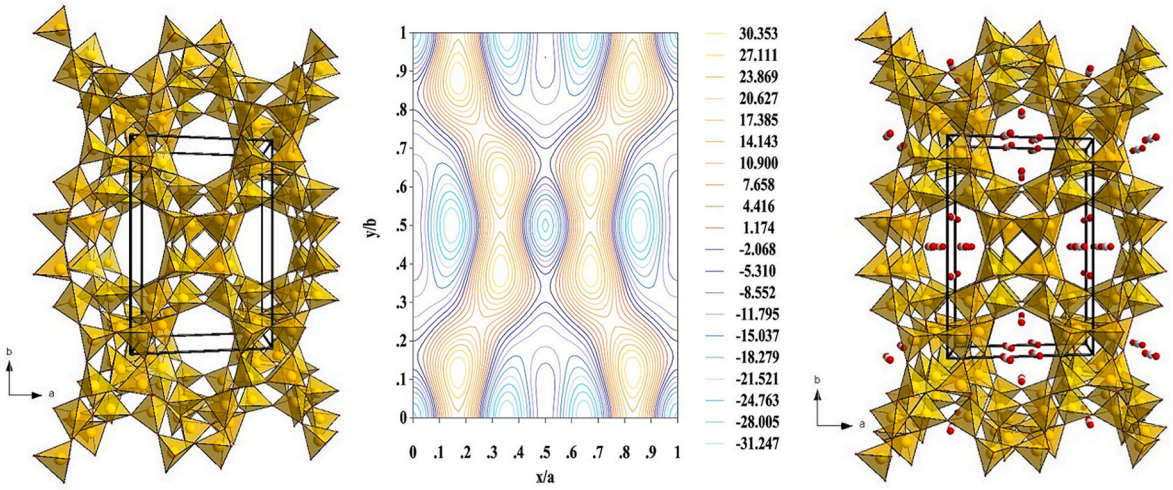

Fig. 12. (left) the projection of empty pure-SiO_2 ITW zeolite framework structure based on corner-connected [SiO_4] tetrahedral groups, (middle) Bidimensional difference Fourier map perpendicular to the c axis in CO_2-filled ITW framework calculated using X-ray structure factors and (right) View of the CO_2-loaded pure-SiO_2 ITW structure along the c axis showing the location of CO_2 molecules at 0.9 GPa. Yellow, gray, and red spheres represent Si, C, and O atoms, respectively.

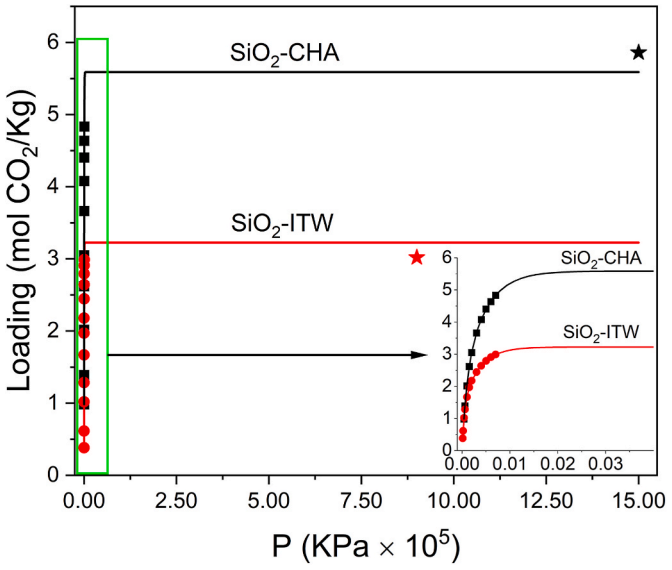

Fig. 13. The CO_2 adsorption isotherms at room temperature of the pure silica CHA and ITW zeolites with the extrapolation of the adsorption CO_2 isotherms measured up to 700 KPa at ambient temperature [11] to our lowest measured pressure points. The inset shows a zoom of the area highlighted with the green rectangle and illustrates the extrapolation of CO_2 isotherm which is based on its asymptotic behavior at low pressures [11], fitted with a two-phase exponential growth function (solid lines). The star scatter points are the experimental data of the present study corresponding to CHA (black) and ITW (red) zeolites.

Declaration of competing interest

The authors declare that they have no known competing financial interests or personal relationships that could have appeared to influence the work reported in this paper.

Data availability

Data will be made available on request.

Acknowledgements

This research was funded by the Spanish Research Agency (AEI) and Spanish Ministry of Science and Investigation (MCIN) (MCIN/AEI/10.13039/501100011033) under projects PGC2021-125518NB-I00, PID2022-138076NB-C41/42, and RED2022-134388-T (cofinanced by EU FEDER funds) as well as by the Generalitat Valenciana under projects CIAICO/2021/241, CIPROM/2021/075 (GREENMAT), and MFA/2022/007 (funded by the European Union—Next Generation EU). This study forms part of the Advanced Materials program and is supported by MCIN with funding from European Union Next Generation EU (PRTR-C17.I1) and by the Generalitat Valenciana. A.O.R. thanks the Principality of Asturias (FICYT), project AYUD/2021/51036 cofinanced by EU FEDER. The authors also thank the MALTA Consolider supercomputing centre and Compute Canada for computational resources and the Elettra Synchrotron Radiation facilities for providing beam-time under the proposal 20225011 and 20230054. The authors thankfully acknowledge the computer resources at MareNostrum5 and the technical support provided by BSC (RES-AECT-2024-2-0010).

Appendix A. Supplementary data

Supplementary data to this article can be found online at https://doi.org/10.1016/j.micromeso.2024.113317.

References

[1] A.A. Olajire, CO_2 capture and separation technologies for end-of-pipe applications–a review, Energy 35 (6) (2010) 2610–2628.
[2] M.K. Mondal, H.K. Balsora, P. Varshney, Progress and trends in CO_2 capture/separation technologies: a review, Energy 46 (1) (2012) 431–441.
[3] F. Zhu, J. Landon, K. Liu, FAU zeolite membranes for dewatering of amine-based post-combustion CO_2 capture solutions, AIChE J. 66 (11) (2020) 17042.
[4] T.R. Anderson, E. Hawkins, P.D. Jones, CO_2, the greenhouse effect and global warming: from the pioneering work of Arrhenius and Callendar to today's Earth System Models, Endeavour 40 (3) (2016) 178–187.
[5] B. Dziejarski, J. Serafin, K. Andersson, R. Krzyżyńska, CO_2 capture materials: a review of current trends and future challenges, Materials Today Sustainability 24 (2023) 100483.
[6] A.I. Osman, M. Hefny, M.I.A. Abdel Maksoud, A.M. Elgarahy, D.W. Rooney, Recent advances in carbon capture storage and utilisation technologies: a review, Environ. Chem. Lett. 19 (2) (2021) 797–849.
[7] S.J. Chen, Y. Fu, Y.X. Huang, Z.C. Tao, M. Zhu, Experimental investigation of CO_2 separation by adsorption methods in natural gas purification, Appl. Energy 179 (2016) 329–337.
[8] R.S. Haszeldine, Carbon capture and storage: how green can black be? Science 325 (2009) 1647–1652.

[9] M.E. Boot-Handford, J.C. Abanades, E.J. Anthony, M.J. Blunt, S. Brandani, N. Mac Dowell, J.R. Fernández, M.C. Ferrari, R. Gross, J.P. Hallett, R.S. Haszeldine, Carbon capture and storage update, Energy Environ. Sci. 7 (1) (2014) 130–189.

[10] W. Rahmah, G.T.M. Kadja, M.H. Mahyuddin, A.G. Saputro, H.K. Dipojono, I. G. Wenten, Small-pore zeolite and zeotype membranes for CO_2 capture and sequestration–A review, J. Environ. Chem. Eng. 10 (6) (2022) 108707.

[11] E. Pérez-Botella, M. Palomino, G.B. Báfero, H.O. Pastore, S. Valencia, F. Rey, The influence of zeolite pore topology on the separation of carbon dioxide from methane, J. CO2 Util. 72 (2023) 102490.

[12] S. Kumar, R. Srivastava, J. Koh, Utilization of zeolites as CO_2 capturing agents: advances and future perspectives, J. CO2 Util. 41 (2020) 101251.

[13] H. Liu, X. Gao, S. Wang, Z. Hong, X. Wang, X. Gu, SSZ-13 zeolite membranes on four-channel α-Al_2O_3 hollow fibers for CO_2 separation, Separ. Purif. Technol. 267 (2021) 118611.

[14] E. Kim, S. Hong, E. Jang, J.H. Lee, J.C. Kim, N. Choi, C.H. Cho, J. Nam, S.K. Kwak, A.C.K. Yip, J. Choi, An oriented, siliceous deca-dodecasil 3R (DDR) zeolite film for effective carbon capture: insight into its hydrophobic effect, J. Mater. Chem. A 5 (2017) 11246–11254.

[15] P. Karakiliç, X. Wang, F. Kapteijn, A. Nijmeijer, L. Winnubst, Defect-free high-silica CHA zeolite membranes with high selectivity for light gas separation, J. Membr. Sci. 586 (2019) 34–43.

[16] A.F. Ismail, K. Khulbe, T. Matsuura, Gas Separation Membranes: Polymeric and Inorganic, Springer, 2015. ISBN 3319010956.

[17] T.D. Pham, R.F. Lobo, Adsorption equilibria of CO_2 and small hydrocarbons in AEI-, CHA-, STT, and RRO-type siliceous zeolites, Microporous Mesoporous Mater. 236 (2016) 100–108.

[18] E.J. García, J. Pérez-Pellitero, C. Jallut, G.D. Pirngruber, Quantification of the confinement effect in microporous materials, Phys. Chem. Chem. Phys. 15 (2013) 5648–5657.

[19] J. Shang, G. Li, R. Singh, Q. Gu, K.M. Nairn, T.J. Bastow, N. Medhekar, C. M. Doherty, A.J. Hill, J.Z. Liu, P.A. Webley, Discriminative separation of gases by a "molecular trapdoor" mechanism in chabazite zeolites, J. Am. Chem. Soc. 134 (2012) 19246–19253.

[20] E.L. Bruce, V.M. Georgieva, M.C. Verbraeken, M.C. Murray, M.F. Hsieh, W. J. Casteel, A. Turrina, S. Brandani, P.A. Wright, Structural chemistry, flexibility, and CO_2 adsorption performance of alkali metal forms of merlinoite with a framework Si/Al ratio of 4.2, J. Phys. Chem. C 125 (2021) 27403–27419.

[21] J.G. Min, K.C. Kemp, H. Lee, S.B. Hong, CO_2 adsorption in the RHO family of embedded isoreticular zeolites, J. Phys. Chem. C 122 (2018) 28815–28824.

[22] E.W. Corcoran Jr., A. Corma, F. Rey, S. Valencia, A. Cantin, M. Palomino, Separation, storage and catalytic conversion of fluids using ITQ-55. WO 2015/196023 A1, 2015.

[23] T.M. Arruda, M. Heon, V. Presser, P.C. Hillesheim, S. Dai, Y. Gogotsi, S.V. Kalinin, N. Balke, In situ tracking of the nanoscale expansion of porous carbon electrodes, Energy Environ. Sci. 6 (1) (2013) 225–231.

[24] D.M. D'Alessandro, B. Smit, J.R. Long, Carbon dioxide capture: prospects for new materials, Angew. Chem. Int. Ed. 49 (35) (2010) 6058–6082.

[25] D. Santamaria-Perez, T. Marqueño, S. MacLeod, J. Ruiz-Fuertes, D. Daisenberger, R. Chulia-Jordan, D. Errandonea, J.L. Jorda, F. Rey, C. McGuire, A. Mahkluf, A. Kavner, C. Popescu, Structural evolution of CO_2-filled pure silica LTA zeolite under high-pressure high-temperature conditions, Chem. Mater. 29 (2017) 4502–4510.

[26] T. Marqueño, D. Santamaria-Perez, J. Ruiz-Fuertes, R. Chulia-Jordan, J.L. Jorda, F. Rey, C. McGuire, A. Kavner, S. MacLeod, D. Daisenberger, C. Popescu, An ultrahigh CO_2-loaded silicalite-1 zeolite: structural stability and physical properties at high pressures and temperatures, Inorg. Chem. 57 (11) (2018) 6447–6455.

[27] J. Haines, O. Cambon, C. Levelut, M. Santoro, F. Gorelli, G. Garbarino, Deactivation of pressure-induced amorphization in silicalite SiO_2 by insertion of guest species, J. Am. Chem. Soc. 132 (2010) 8860–8861.

[28] J.M. Thibaud, J. Rouquette, P. Hermet, K. Dziubek, F.A. Gorelli, M. Santoro, G. Garbarino, F.G. Alabarse, O. Cambon, F. Di Renzo, A. Van der Lee, J. Haines, High-pressure phase transition, pore collapse, and amorphization in the siliceous 1D zeolite, TON. J. Phys. Chem. C. 121 (8) (2017) 4283–4292.

[29] G.D. Gatta, Y. Lee, Zeolites at high pressure: a review, Mineral. Mag. 78 (2) (2014) 267–291.

[30] S. Fujiyama, N. Kamiya, K. Nishi, Y. Yokomori, Adsorption process of CO_2 on silicalite-1 zeolite using single-crystal x-ray method, Langmuir 30 (2014) 3749–3753.

[31] S. Fujiyama, N. Kamiya, K. Nishi, Y. Yokomori, Reanalysis of CO_2-silicalite-1 structure as monoclinic twinning, Z. für Kristallogr. - Cryst. Mater. 229 (2014) 303–309.

[32] A. Hirotani, K. Mizukami, R. Miura, H. Takaba, T. Miya, A. Fahmi, A. Stirling, M. Kubo, A. Miyamoto, Grand canonical Monte Carlo simulation of the adsorption of CO_2 on silicalite and NaZSM-5, Appl. Surf. Sci. 120 (1997) 81–84.

[33] R. Babarao, Z. Hu, J. Jiang, S. Chempath, S.I. Sandler, Storage and separation of CO_2 and CH4 in silicalite, C168 schwarzite and IRMOF-1: a comparative study from Monte Carlo simulation, Langmuir 23 (2007) 659–666.

[34] J.L. Jordá, F. Rey, G. Sastre, S. Valencia, M. Palomino, A. Corma, A. Segura, D. Errandonea, R. Lacomba, F.J. Manjón, O. Gomis, A. Kleppe, A.P. Jephcoat, M. Amboage, A. Rodriguez-Velamazan, Synthesis of a novel zeolite through a pressure-induced reconstructive phase transition process, Angew. Chem. Int. Ed. 52 (40) (2013) 10458–10462.

[35] http://www.iza-structure.org/databases/.

[36] M. Palomino, H. Ono, S. Valencia, A. Corma, Preparation of continuous highly hydrophobic pure silica ITQ-29 zeolite layers on alumina supports, Molecules 25 (18) (2020) 4150.

[37] M. Miyamoto, Y. Fujioka, K. Yogo, Pure silica CHA type zeolite for CO2 separation using pressure swing adsorption at high pressure, J. Mater. Chem. 22 (2012) 20186–20189.

[38] M.S. Nobandegani, L. Yu, J. Hedlund, Zeolite membrane process for industrial CO_2/CH_4 separation, Chem. Eng. J. 446 (4) (2022) 137223.

[39] A. Rojas, E. Martinez-Morales, C.M. Zicovich-Wilson, M.A. Camblor, Zeolite synthesis in fluoride media: structure direction toward ITW by small methylimidazolium cations, J. Am. Chem. Soc. 134 (4) (2012) 2255–2263.

[40] M.J. Díaz-Cabañas, P.A. Barret, M.A. Camblor, Synthesis and structure of pure SiO_2 chabazite: the SiO_2 polymorph with the lowest framework density, Chem. Commun. (1998) 1881–1882.

[41] P.A. Barrett, T. Boix, M. Puche, D.H. Olson, E. Jordan, H. Koller, M.A. Camblor, ITQ-12: a new microporous silica polymorph potentially useful for light hydrocarbon separations, Chem. Commun. (2003) 2114–2115.

[42] T. Boix, M. Puche, M.A. Camblor, A. Corma, U.S. Patent 6 (2002), 471, 939.

[43] D. Santamaria-Perez, C. McGuire, A. Makhluf, A. Kavner, R. Chulia-Jordan, J. Pellicer-Porres, D. Martinez-Garcia, A. Doran, M. Kunz, P. Rodriguez-Hernandez, A. Muñoz, Exploring the chemical reactivity between carbon dioxide and three transition metals (Au, Pt, and Re) at high-pressure, high-temperature conditions, Inorg. Chem. 55 (2016) 10793–10799.

[44] D. Santamaria-Perez, C. McGuire, A. Makhluf, A. Kavner, R. Chulia-Jordan, J. L. Jorda, F. Rey, J. Pellicer-Porres, D. Martinez-Garcia, P. Rodriguez-Hernandez, A. Muñoz, Strongly-driven Re + CO2 redox reaction at high-pressure and high-temperature, Nat. Commun. 7 (2016) 13647.

[45] R. Chulia-Jordam, D. Santamaria-Perez, T. Marqueño, J. Ruiz-Fuertes, D. Daisenberger, Oxidation of high yield strength metals tungsten and rhenium in high-pressure high-temperature experiments of carbon dioxide and carbonates, Crystals 9 (2019) 676.

[46] K.K. Mao, J. Xu, P.M. Bell, Calibration of the ruby pressure gauge to 800-kbar under quasi-hydrostatic conditions, J. Geophys. Res. 91 (1986) 4673–4676.

[47] V.M. Giordano, F. Datchi, F. Gorelli, R. Bini, Equation of state and anharmonicity of carbon dioxide phase I up to 12 GPa and 800 K, J. Chem. Phys. 133 (2010) 144501.

[48] C. Prescher, V.B. Prakapenka, DIOPTAS: a program for reduction of two-dimensional X-ray diffraction data and data exploration, High Pres. Res. 35 (2015) 223–230.

[49] T.J.B. Holland, S.A.T. Redfern, Unit cell refinement from powder diffraction data: the use of regression diagnostics, Mineral. Mag. 61 (1997) 65–77.

[50] G. Nolze, W. Kraus, Powdercell 2.0 for windows, Powder Diffr. 13 (1998) 256–259.

[51] J. Rodriguez-Carvajal, Recent advances in magnetic structure determination by neutron powder diffraction, Physica B 192 (1993) 55–69.

[52] V. Blum, R. Gehrke, F. Hanke, P.V. Havu Havu, X. Ren, K. Reuter, M. Scheffler, Ab initio molecular simulations with numeric atom-centered orbitals, Comput. Phys. Commun. 180 (2009) 2175–2196.

[53] V. Havu, V. Blum, P. Havu, M. Scheffler, Efficient O(N) integration for all-electron electronic structure calculation using numerically tabulated basis functions, J. Comput. Phys. 238 (2009) 8367–8379.

[54] A.D. Becke, On the large-gradient behavior of the density functional exchange energy, J. Chem. Phys. 85 (1986) 7184–7187.

[55] J.P. Perdew, K. Burke, M. Ernzerhof, Generalized gradient approximation made simple, Phys. Rev. Lett. 77 (1996) 3865–3868.

[56] E.R. Johnson, The exchange-hole dipole moment dispersion model, in: A. Otero-de-la-Roza, G.A. DiLabio (Eds.), Non-covalent Interactions in Quantum Chemistry and Physics, Elsevier, 2017, pp. 169–194 (Chapter 5).

[57] A.D. Becke, E.R. Johnson, Exchange-hole dipole moment and the dispersion interaction revisited, J. Chem. Phys. 127 (2007) 154108–154114.

[58] A. Otero-De-La-Roza, E.R. Johnson, Van der Waals interactions in solids using the exchange-hole dipole moment model, J. Chem. Phys. 136 (2012) 174109.

[59] A.J.A. Price, A. Otero-de-la-Roza, E.R. Johnson, XDM-corrected hybrid DFT with numerical atomic orbitals predicts molecular crystal lattice energies with unprecedented accuracy, Chem. Sci. 14 (2023) 1252.

[60] F. Birch, Finite elastic strain of cubic crystals, Phys. Rev. 71 (1947) 809.

[61] Julien Haines, Olivier Cambon, Claire Levelut, Mario Santoro, Federico Gorelli, Gaston Garbarino, Deactivation of pressure-induced amorphization in silicalite SiO2 by insertion of guest species, J. Am. Chem. Soc. 132 (26) (2010) 8860–8861.

[62] Jason Richard, Sonia León Cid, Jérôme Rouquette, Arie van der Lee, Samuel Bernard, Haines Julien, Pressure-induced insertion of ammonia borane in the siliceous zeolite, silicalite-1F, J. Phys. Chem. C 120 (17) (2016) 9334–9340.

[63] R.M. Hazen, L.W. Finger, Compressibility of zeolite 4A is dependent on the molecular size of the hydrostatic pressure medium, J. Appl. Phys. 56 (1984) 1838–1840.

[64] R.J. Angel, Equations of state, Rev. Mineral. Geochem. 41 (2000) 35–59.

[65] Datchi, Frédéric, G. Weck, A. M. Saitta, Zamaan Raza, G. Garbarino, S. Ninet, D. K. Spaulding, J. A. Queyroux, and M. Mezouar. "Structure of liquid carbon dioxide at pressures up to 10 GPa." Physical Review B 94, no. 1 (2016): 014201.

[66] Giordano, Valentina M., Frédéric Datchi, Federico A. Gorelli, and Roberto Bini. "Equation of state and anharmonicity of carbon dioxide phase I up to 12 GPa and 800 K." The Journal of chemical physics 133, no. 14 (2010).

[67] B. Qu, D. Li, L. Wang, R. Zhou, B. Zhang, X.-C. Zeng, J. Wu, Mechanistic study of pressure and temperature dependent structural changes in reactive formation of silicon carbonate, RSC Adv 6 (2016) 26650–26657.